Spin-Nernst effect in the paramagnetic regime of an antiferromagnetic insulator

Yinhan Zhang, Satoshi Okamoto, and Di Xiao

Spin Nernst effect in the Paramagnetic Regime of An Antiferromagnetic Insulator

Yinhan Zhang,[1] Satoshi Okamoto,[2] and Di Xiao[1]

[1]*Department of Physics, Carnegie Mellon University, Pittsburgh, Pennsylvania 15213, USA*
[2]*Materials Science and Technology Division, Oak Ridge National Laboratory, Oak Ridge, Tennessee 37831, USA*
(Dated: July 5, 2018)

We theoretically investigate a pure spin Hall current driven by a longitudinal temperature gradient, i.e. the spin Nernst effect (SNE), in a paramagnetic state of a collinear antiferromagnetic insulator with the Dzyaloshinskii-Moriya interaction. The SNE in a magnetic ordered state in such an insulator was proposed by Cheng *et al.* [PRL 117, 217202 (2016)]. Here we show that the Dzyaloshinskii-Moriya interaction can generate a pure spin Hall current even without magnetic ordering. By using a Schwinger boson mean-field theory, we calculate the temperature dependence of SNE in a disordered phase. We also discuss the implication of our results to experimental realizations.

I. INTRODUCTION

Recent years have seen a surge of interest in issues related to spin transport in magnetic insulators. For practical purposes, the ability to transfer spin information in the absence of charge flow holds great potential for energy-efficient applications [1–9]. On the fundamental side, spin transport measurements can also provide valuable information about the ground state and low-energy excitations of correlated electronic systems [10]. In particular, a thermal Hall effect (THE) of spin excitations has been predicted [11]. In this effect, a longitudinal temperature gradient can drive a transverse heat current carried by charge-neutral excitations such as magnons or spinons. Since its prediction, the THE has been observed in a number of magnetic insulators [12–15], accompanied by extensive theoretical efforts [16–24]. It is now recognized that, microscopically, the THE originates from nontrivial magnon dispersions due to either chiral spin textures or non-symmetric spin-spin interactions, such as the Dzyaloshinskii-Moriya interaction (DMI).

However, in certain class of magnetic insulators, the THE is symmetry prohibited. Examples include magnetically disordered states at high temperatures and collinear antiferromagnets with combined time-reversal ($\mathcal{T}$) and inversion ($\mathcal{I}$) symmetry. For these systems, a spin Nernst effect (SNE) is symmetry allowed nonetheless. In the SNE, spin currents with opposite polarization flow in the opposite transverse direction in response to a longitudinal temperature gradient. As a result, the heat current vanishes, and we are left with a pure transverse spin current. The relation between the THE and the SNE is akin to the relation between the anomalous Hall effect and the spin Hall effect. The SNE has been predicted for magnets on a honeycomb lattice, either in antiferromagnets (AFM) below the Néel temperature in which the SNE is realized by magnons [25–27], or ferromagnets (FM) above the Curie temperature in which the SNE is realized by spinons [28]. Possible experimental signature of the SNE has also been reported in the antiferromagnetic insulator $MnPS_3$ in the ordered phase [29].

Actually, the honeycomb magnets can display either

the THE or the SNE depending on their magnetic configurations, as summarized in Table I. The key ingredient here is a second nearest-neighbor DMI, which plays a similar role in spin transport as the spin-orbit interaction in electron transport. In the ordered phase of a honeycomb FM, the broken time-reversal symmetry together with the DMI leads to the THE [22, 28]. On the other hand, in both the disordered phase of the FM and the ordered phase of the AFM, the vanishing magnetization forbids the THE, but the DMI still allows the SNE [25, 26, 28]. These results strongly hint that the SNE should also exist in the high-temperature disordered phase of the honeycomb AFM.

In this paper we present a detailed study of this effect using the Schwinger boson mean-field approach. We show that the SNE is indeed enabled by the DMI in the high-temperature disordered phase of a honeycomb AFM, and the transverse spin current is carried by the two pairs of conjugated spinon states connected by the combined $\mathcal{T}\mathcal{I}$ symmetry. Supplemented by a symmetry analysis, we calculate the reduced mean-field order parameters of the spinons, establish the disordered phase regime, and then identify the effect of a $\mathcal{T}\mathcal{I}$ conjugate pair on the pure SNE. Finally, we calculate the temperature dependence of the SNE coefficient in this disordered phase, and discuss its realization in real materials.

This paper is organized as follows. In Sec. II, we introduce the honeycomb AFM model with a second nearest neighbor DMI, and present the mean-field solution to the

collinear order	ordered	disordered
FM	THE [a]	SNE [b]
AFM	SNE [c]	SNE [d]

[a] Ref. 22 and 28.
[b] Ref. 28.
[c] Ref. 25 and 26.
[d] This work.

TABLE I. Summary of the thermal Hall effect (THE) and the spin Nernst effect (SNE) in honeycomb magnets with a second nearest-neighbor Dzyaloshinskii-Moriya interaction. Depending on the symmetry, the system exhibits either a THE or a SNE.
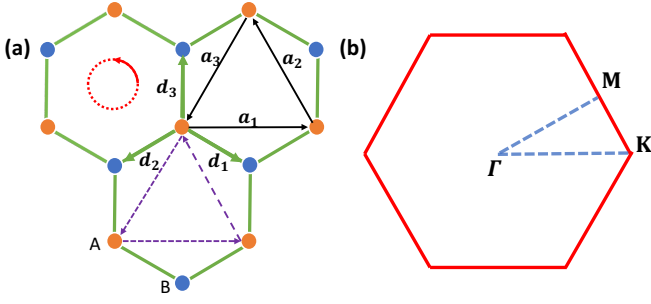
FIG. 1. (a) An AFM honeycomb with DMI. The lattice vectors are $\boldsymbol{a}_1$, $\boldsymbol{a}_2$, and $\boldsymbol{a}_3$, and the nearest bond vectors are $\boldsymbol{d}_1$, $\boldsymbol{d}_2$ and $\boldsymbol{d}_3$. (b) The corresponding hexagonal Brillouin zone.

Schwinger boson Hamiltonian. This is followed by a discussion of the SNE in Sec. III, including its dependence on the temperature, the staggered field, and the DMI strength. Finally, we comment on the limitations of our theoretical treatment and discuss possible material realizations of the SNE in Sec. IV.

II. MODEL AND METHOD

A. Honeycomb AFM

We begin with the following spin Hamiltonian on a honeycomb lattice,

$$
H = J_1 \sum_{\langle i,j \rangle} \boldsymbol{S_i} \cdot \boldsymbol{S_j} + D_2 \sum_{\langle\langle i,j \rangle\rangle} v_{ij} \hat{z} \cdot (\boldsymbol{S_i} \times \boldsymbol{S_j}) \\
- h_{st} \sum_i (-1)^i S_i^z .
\tag{1}
$$

The first term describes the antiferromagnetic nearest-neighbor (NN) Heisenberg exchange with $J_1 > 0$. The second term is a second-NN DMI. Here $v_{ij} = 2\sqrt{3}(\boldsymbol{d}_1 \times \boldsymbol{d}_2)_z = \pm 1$ with $\boldsymbol{d}_1$ and $\boldsymbol{d}_2$ the vectors connecting site i to its second NN site j, as shown in Fig. 1. This second-NN DMI is allowed by crystal symmetry [30, 31]; it is intrinsic to the honeycomb lattice. The third term is a staggered Zeeman field along the z-direction that stabilizes the system in the collinear AFM ground state at low temperatures [32]. Throughout this paper, we will use J_1 as the energy and temperature unit.

In the high-temperature paramagnetic (PM) phase, the low-energy spin dynamics can be described by spinons. We introduce the Schwinger boson (SB) representation for the spin operator [34]

$$
\boldsymbol{S}_i \equiv \frac{1}{2} \sum_{s,s'} c_{i,s}^\dagger \boldsymbol{\sigma}_{ss'} c_{i,s'}, \quad (s,s' = \pm 1)
\tag{2}
$$

with the constraint that the number of spinons must be conserved at any given site, $\sum_s c_{i,s}^\dagger c_{i,s} = 2S$. The index $s = \pm 1$ denotes up or down spins. In Eq. (2), $\boldsymbol{\sigma}$ are

the Pauli matrices, and $c_{i,s}^\dagger$ ($c_{i,s}$) denotes the creation (annihilation) operator for a spinon with spin s at site i. The spin amplitude $S = 1/2$ is considered in this paper.

Substituting Eq. (2) into the spin Hamiltonian (1), we obtain

$$
H_{\mathrm{SB}} = -2J_1 \sum_{\langle i,j \rangle} \vec{\mathcal{A}}_{ij}^\dagger \vec{\mathcal{A}}_{ij} - \frac{iD_2}{2} \sum_{\langle\langle i,j \rangle\rangle} \sum_s s v_{ij} \mathcal{F}_{ij,s}^\dagger \mathcal{F}_{ij,-s} \\
- h_{st} \sum_{is} \frac{(-1)^i}{2} s c_{i,s}^\dagger c_{i,s} + \sum_i \mu_i \Big(\sum_s c_{i,s}^\dagger c_{i,s} - 2S \Big).
\tag{3}
$$

where $\vec{\mathcal{A}}_{ij} \equiv (c_{i,\uparrow} c_{j,\downarrow} - c_{i,\downarrow} c_{j,\uparrow})/2$ is the antiferromagnetic NN bond operator, and $\mathcal{F}_{ij,s} \equiv c_{is}^\dagger c_{js}$ is the second NN bond operator. μ_i is a Lagrange multiplier to impose the local constraint at the mean field level. We note that $\vec{\mathcal{A}}_{ij} = -\vec{\mathcal{A}}_{ji}$ is antisymmetric. Next we perform the mean-field decomposition of the quartic terms of the spinon Hamiltonian. For the NN bond operator, we set $\langle \vec{\mathcal{A}}_{ij} \rangle = -\langle \vec{\mathcal{A}}_{ji} \rangle = \chi_{ij}$. While in general χ_{ij} is complex, we work in the gauge in which χ_{ij} is real. The second-NN order parameter can be written as $\langle \mathcal{F}_{ij,s} \rangle \equiv \eta_{ij,s}^S + i v_{ij} \eta_{ij,s}^A = \eta_{ij,s}$, where $\eta_{ij,s}^S = \langle \mathcal{F}_{ij,s} + \mathcal{F}_{ji,s} \rangle/2$, and $\eta_{ij,s}^A = v_{ij} \langle \mathcal{F}_{ij,s} - \mathcal{F}_{ji,s} \rangle/(2i)$. The resulting bosonic Bogoliubovde Gennes (BdG) Hamiltonian is given by

$$
H_{SB}^M = -J_1 \sum_{\langle i,j \rangle} \sum_s \Big(s \chi_{ij} c_{i,s}^\dagger c_{j,-s}^\dagger + h.c. \Big) \\
+ D_2 \sum_{\langle\langle i,j \rangle\rangle} \sum_s \frac{i v_{ij}}{2} s \eta_{ij,-s}^S \Big(c_{i,s}^\dagger c_{j,s} - h.c. \Big) \\
+ D_2 \sum_{\langle\langle i,j \rangle\rangle} \sum_s \frac{s}{2} \eta_{ij,-s}^A \Big(c_{i,s}^\dagger c_{j,s} + h.c. \Big) \\
+ \sum_{is} (\mu_i - \frac{(-1)^i h_{st}}{2} s) c_{i,s}^\dagger c_{i,s},
\tag{4}
$$

where the trivial constant terms such as $2J_1 \sum_{\langle i,j \rangle} \chi_{ij}^2$ are neglected for simplicity.

This Hamiltonian can be simplified by symmetry considerations. The spin Hamiltonian (1) has the combined $\mathcal{TI}$ symmetry, which persists even in the low temperature AFM phase. Therefore, it is natural to expect that the high-temperature PM phase also preserves the $\mathcal{TI}$ symmetry. For the purpose of symmetry analysis, it is convenient to introduce sublattice-specific notations. We use $a_{i,s}$ and $b_{i,s}$ to denote the annihilation operators on the A and B sublattices, respectively. The corresponding second NN bond order parameter is then denoted by $A_{ij,s}$ and $B_{ij,s}$. The $\mathcal{T}$ and $\mathcal{I}$ symmetry are defined as [35] (more details in Appendix A)

$$
\mathcal{T} c_{i,s} \mathcal{T}^{-1} = i(\sigma_2)_{s,s'} c_{i,s'},
\tag{5}
$$

$$
\mathcal{I} \begin{bmatrix} a_i \\ b_i \end{bmatrix} \mathcal{I}^{-1} = \sigma_3 \sigma_1 \begin{bmatrix} a_{-i} \\ b_{-i} \end{bmatrix}.
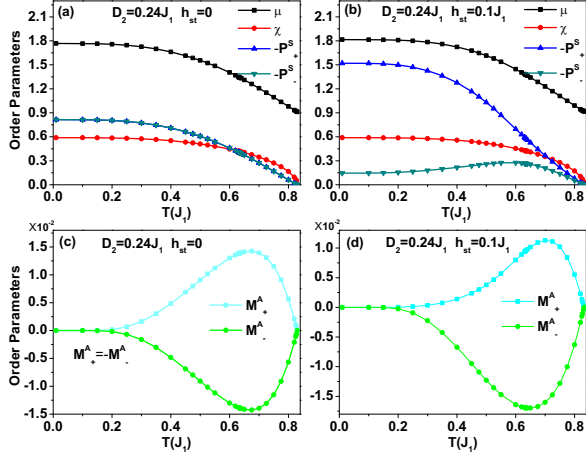\tag{6}
$$

FIG. 2. The solution of order parameters with staggered field $h_{st} = 0$ for (a) and (c), and $h_{st} = 0.1J_1$ for (b) and (d).
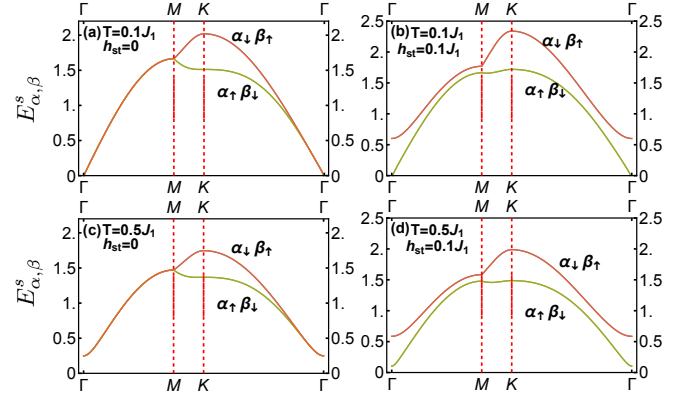

FIG. 3. The dispersions along high symmetry lines $\Gamma - M - K - \Gamma$ for (a) $h_{st} = 0$ and $T = 0.1J_1$, (b) $h_{st} = 0.1J_1$ and $T = 0.1J_1$, (c) $h_{st} = 0$ and $T = 0.5J_1$, and (d) $h_{st} = 0.1J_1$ and $T = 0.5J_1$. $\alpha(\beta)_{\uparrow(\downarrow)}$ denotes the mode $E^s_{\alpha(\beta)}(\boldsymbol{k})$ with $s = \pm 1$ for spin $\uparrow (\downarrow)$.

Imposing the $\mathcal{TI}$ symmetry on the mean-field Hamiltonian (4) yields

$$A^*_{ij,-s} = B_{-i-j,s} . \tag{7}$$

We now assume that the bond order parameters and the chemical potential are spatially uniform. They are $A_{ij,s} = A^S_s + iv_{ij}A^A_s$, $B_{ij,s} = B^S_s + iv_{ij}B^A_s$, $\chi_{ij} = \chi_0$ and $\mu_i = \mu$. Fourier transforming into the momentum space $\Psi_{\boldsymbol{k}s} = [a_{\boldsymbol{k},s}, b^\dagger_{-\boldsymbol{k},-s}]^T = (1/\sqrt{N}) \sum_i e^{-i\boldsymbol{k}\cdot\boldsymbol{R}_i}[a_{i,s}, b^\dagger_{i,-s}]^T$, and using the condition (7), we obtain the mean-field spinon Hamiltonian in the momentum space

$$H^M_{SB} = \sum_{\boldsymbol{k},s,\mu} \Psi^\dagger_{\boldsymbol{k}s} h^s_\mu(\boldsymbol{k})\sigma_\mu \Psi_{\boldsymbol{k}s}, \tag{8}$$

where $\sigma_\mu = \{I_{2\times 2}, \sigma_x, \sigma_y, \sigma_z\}$ and

$$h^s_0(\boldsymbol{k}) = \mu - s\frac{h_{st}}{2} + \frac{D_2 s}{4}M^A_{-s}g_S(\boldsymbol{k}), \tag{9a}$$

$$h^s_1(\boldsymbol{k}) - ih^s_2(\boldsymbol{k}) = -J_1\chi_0 sf(\boldsymbol{k}), \tag{9b}$$

$$h^s_3(\boldsymbol{k}) = \frac{D_2 s}{4}P^S_{-s}g_A(\boldsymbol{k}). \tag{9c}$$

with $M^A_s \equiv A^A_s - B^A_{-s}$ and $P^S_s \equiv A^S_s + B^S_{-s}$. The structure factors are $g_A(\boldsymbol{k}) \equiv -2\sum_i \sin(\boldsymbol{k}\cdot\boldsymbol{a}_i)$, $g_S(\boldsymbol{k}) \equiv 2\sum_i \cos(\boldsymbol{k}\cdot\boldsymbol{a}_i)$, and $f(\boldsymbol{k}) = \sum_i e^{i\boldsymbol{d}_i\cdot\boldsymbol{k}}$. $g_A(\boldsymbol{k})$ is an odd function of $\boldsymbol{k}$, and $g_S(\boldsymbol{k})$ and $|f(\boldsymbol{k})|$ are even functions of $\boldsymbol{k}$.

B. Schwinger Boson mean-field solution

The spinon Hamiltonian (8) contains six parameters that need to be determined self-consistently, namely, μ, χ_0, and M^A_s and P^S_s (with $s = \pm 1$). To diagonalize the Hamiltonian (8), we perform the Bogoliubov transformation $\Phi_{\boldsymbol{k},s} = U^{-1}_s(\boldsymbol{k})\Psi_{\boldsymbol{k},s} = [\alpha_{\boldsymbol{k},s}, \beta^\dagger_{-\boldsymbol{k},-s}]^T$, where

$U^{-1}_s(\boldsymbol{k})$ is a paraunitary matrix given by

$$U^{-1}_s(\boldsymbol{k}) = \begin{bmatrix} \cosh\frac{\theta_s(\boldsymbol{k})}{2} & \sinh\frac{\theta_s(\boldsymbol{k})}{2}e^{-i\varphi_s(\boldsymbol{k})} \\ \sinh\frac{\theta_s(\boldsymbol{k})}{2}e^{i\varphi_s(\boldsymbol{k})} & \cosh\frac{\theta_s(\boldsymbol{k})}{2} \end{bmatrix} . \tag{10}$$

Here the Bogoliubov angles θ and φ are defined by h^s in Eq. (9): $h^s_1 = h^s\sinh\theta_s\cos\varphi_s$, $h^s_2 = h^s\sinh\theta_s\sin\varphi_s$ and $h^s_0 = h^s\cosh\theta_s$, with $h^s \equiv \sqrt{h^{s2}_0 - h^{s2}_1 - h^{s2}_2}$. The diagonalized Hamiltonian has the form $H^M_{SB} = \sum_{\boldsymbol{k}s}(E^s_\alpha(\boldsymbol{k})\alpha^\dagger_{\boldsymbol{k}s}\alpha_{\boldsymbol{k}s} + E^s_\beta(\boldsymbol{k})\beta^\dagger_{\boldsymbol{k}s}\beta_{\boldsymbol{k}s})$. It is clear that H^M_{SB} has two degenerate modes with $E^s_\alpha(\boldsymbol{k}) = E^{-s}_\beta(\boldsymbol{k}) = h^s(\boldsymbol{k}) + h^s_3(\boldsymbol{k})$,

$$E^s_\alpha(\boldsymbol{k}) = \frac{D_2 s}{4}P^S_{-s}g_{A\boldsymbol{k}}$$
$$+ \sqrt{(\mu - s\frac{h_{st}}{2} + \frac{D_2 s}{4}M^A_{-s}g_{S\boldsymbol{k}})^2 - |J_1\chi_0 f_{\boldsymbol{k}}|^2} . \tag{11}$$

The wave function of the $\alpha_{\boldsymbol{k}s}$ ($\beta_{\boldsymbol{k}s}$) quasiparticle are given in Appendix C.

This degeneracy originates from the combined $\mathcal{TI}$ symmetry of our mean-field Hamiltonian. We note that the annihilation operator of a spinon $\alpha_{\boldsymbol{k}s}$ transforms into into $s\beta_{\boldsymbol{k},-s}$ under the $\mathcal{TI}$ operation defined in Eq. (5). From this, we find

$$E^s_\alpha(\boldsymbol{k}) = E^{-s}_\beta(\boldsymbol{k}) . \tag{12}$$

We call such a pair of degenerate modes as a $\mathcal{TI}$ symmetry conjugate pair. This conjugate pair is crucial for the appearance of a pure transverse spin current as we discuss below.

We compute mean-field order parameters by solving a set of self-consistent equations detailed in Appendix B. The temperature dependence of order parameters at $D_2 = 0.24J_1$ with different h_{st} are shown in Fig. 2, along
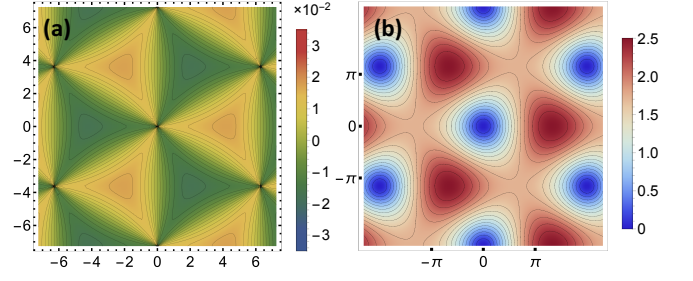
FIG. 4. The distributions of Berry curvature and spectrum for $\alpha_{\boldsymbol{k},s}$ spinon with spin $s = -1$ at temperature $T = 0.1J_1$ without staggered fields: (a) The Berry curvature; (b) The spectrum.

III. SPIN NERNST EFFECT OF SPINONS

A. Spin conservation and mirror symmetry

With a firm understanding of the spinon spectra, we now turn to the SNE. As a first step, we examine how many spins are carried by the spinon modes. In general, this is not a trivial question, because in the presence of the DMI the spin angular momentum does not have to be conserved. Fortunately, our model also has the mirror symmetry $\mathcal{M}_z$ about the lattice plane, which leads to the conservation of the total spin S_z,

$$S_z = \frac{\hbar}{2} \sum_{\boldsymbol{k}s} s \Psi_{\boldsymbol{k}s}^\dagger \sigma_z \Psi_{\boldsymbol{k}s} = \frac{\hbar}{2} \sum_{\boldsymbol{k}s} s \Phi_{\boldsymbol{k}s}^\dagger \sigma_z \Phi_{\boldsymbol{k}s}. \quad (13)$$

We see that $\alpha_{\boldsymbol{k}s}$ and $\beta_{\boldsymbol{k}-s}$ modes have opposite angular momentum $\langle 0|\alpha_{\boldsymbol{k}s} S_z \alpha_{\boldsymbol{k}s}^\dagger|0\rangle = \hbar s/2$ and $\langle 0|\beta_{\boldsymbol{k}-s} S_z \beta_{\boldsymbol{k}-s}^\dagger|0\rangle = -\hbar s/2$, respectively. Here $|0\rangle$ is the vacuum state of spinons. The SNE is due to the opposite transverse motion of the two spin species driven by a longitudinal temperature gradient.

B. Spin Nernst Effect coefficient in disordered state

Since spinons do not carry charge, they cannot be driven by an external electric field, but they can respond to a statistical force, such as the temperature gradient ∇T. Due to the conservation of S_z, spin current can be written as $\boldsymbol{J}^{SN} = \sum_{s,\lambda} s(\hbar/2) \boldsymbol{J}_\lambda^s$, where $\boldsymbol{J}_\lambda^s$ is the spinon current of mode λ and spin s. According to Ref. [16, 17, 20, 25], the transverse $\boldsymbol{J}_\lambda^s$ due to ∇T is given by

$$\boldsymbol{J}_\lambda^s = \frac{\hat{\boldsymbol{z}}}{\hbar} \times \nabla T \int \frac{d\boldsymbol{k}}{(2\pi)^2} c_1(n_s^\lambda(\boldsymbol{k})) \Omega_\lambda^s(\boldsymbol{k}), \quad (14)$$

where c_1 is the weight function $c_1(x) = x \ln x - (1 + x) \ln(1 + x)$, and $n_s^\lambda(\boldsymbol{k})$ and $\Omega_\lambda^s(\boldsymbol{k})$ are the Bose-Einstein distribution function and the Berry curvature (defined below) for the mode $E_\lambda^s(\boldsymbol{k})$, respectively.

We now analyze the symmetry properties of the Berry curvature, which for the mode $E_\alpha^s(\boldsymbol{k})$ is expressed as

$$\Omega_\alpha^s(\boldsymbol{k}) = i\partial_{\boldsymbol{k}} u_\alpha^{s\dagger}(\boldsymbol{k}) \times \sigma_3 \partial_{\boldsymbol{k}} u_\alpha^s(\boldsymbol{k})$$
$$= \frac{1}{2} \nabla_{\boldsymbol{k}} \cosh\theta_s(\boldsymbol{k}) \times \nabla_{\boldsymbol{k}} \varphi_s(\boldsymbol{k}), \quad (15)$$

where $u_\alpha^s(\boldsymbol{k})$ is the wave function of the $\alpha_{\boldsymbol{k},s}$ quasiparticle as presented in Appendix C. Under the $\mathcal{TI}$ operation, $\alpha \to \beta$, $s \to -s$, and $\boldsymbol{k} \to \boldsymbol{k}$. In addition, the Berry curvature should also flip sign due to the factor i in its definition. As such, under the $\mathcal{TI}$ operation, we have

$$\Omega_\beta^{-s}(\boldsymbol{k}) = -\Omega_\alpha^s(\boldsymbol{k}). \quad (16)$$

Together with the energy dispersion relation $E_\alpha^s(\boldsymbol{k}) = E_\beta^{-s}(\boldsymbol{k})$ [see Eq. (12)], this relation indicates that $\boldsymbol{J}_\alpha^s$ and $\boldsymbol{J}_\beta^{-s}$ are always opposite in sign, resulting in a pure transverse spin current.

Next we focus on a particular mode α. For bosonic BdG equations, there is a general relation of the Berry curvature between the α and β mode (See Appendix D)

$$\Omega_\beta^s(\boldsymbol{k}) = \Omega_\alpha^{-s}(-\boldsymbol{k}). \quad (17)$$

Combined this relation with Eq. (16), we have

$$\Omega_\alpha^s(\boldsymbol{k}) = -\Omega_\alpha^s(-\boldsymbol{k}). \quad (18)$$

This is clearly seen in Fig. 4 (a). If the spinon dispersion is inversion symmetric, the transverse current $\boldsymbol{J}_\alpha^s$ would vanish. However, as we can see from Eq. (11), the presence of the DMI breaks this symmetry, i.e., $E_\lambda^s(\boldsymbol{k}) \neq E_\lambda^s(-\boldsymbol{k})$ as illustrated in Fig. 4 (b). After summing over all occupied states, there should be a net spinon current. Therefore the second NN DMI is crucial for the appearance of the SNE.

We numerically calculate the spin Nernst coefficient given by [16, 17, 20, 25]

$$\alpha_{xy} = \sum_s \int \frac{d\boldsymbol{k}}{(2\pi)^2} c_1(n_s^\alpha(\boldsymbol{k})) \Omega_\alpha^s(\boldsymbol{k}). \quad (19)$$

where α_{xy} is defined by the relation $\boldsymbol{J}^{SN} = \alpha_{xy}\hat{\boldsymbol{z}} \times \nabla T$. The temperature dependence of α_{xy} is calculated at different staggered field h_{st} and DMI strength D_2 in Fig. 5.

With the spinon dispersion in Fig. 3. We first note that all order parameters vanish above $T_c \sim 0.826J_1$. This is an artifact of the mean-field approach, and T_c should be interpreted as a characteristic crossover temperature above which the system behaves as a paramagnet with local moments [34]. On the other hand, as the temperature approaches zero, the spinon gap at the Γ point closes (Fig. 3), and the system undergoes a phase transition into the collinear AFM phase at the Néel temperature T_N via the spinon condensation [36].

For the current two-dimensional model, T_N is strictly zero because single-site spin anisotropy or anisotropic exchange coupling is absent. Spin ordering at finite T is mimicked by nonzero staggered field h_{st}.
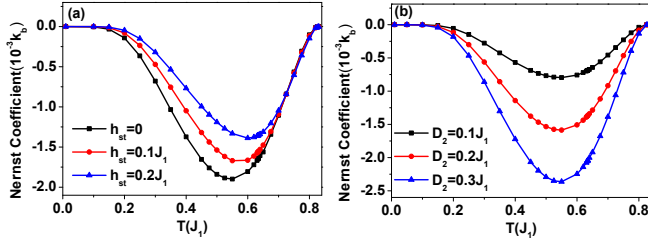
FIG. 5. The spinon Nernst coefficients as a function of temperature: (a) at different staggered fields h_{st} and a fixed DM interaction $D_2 = 0.24J_1$;(b) at different DM interaction D_2 and without a staggered field.
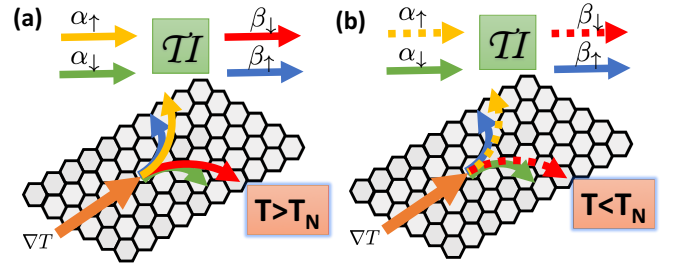

FIG. 6. It illustrates the spin Nernst effect on a honeycomb AFM carried by spin fluctuations: (a) at $T > T_N$, the SNE is carried by spinons in the paramagnetic phase; (b) at $T < T_N$, the SNE is carried by magnons.

We find that α_{xy} will be zero at two ends of the temperature zone, i.e., $T = 0$ and $T = T_c$. When T approaches zero, the fluctuating component of spinons is decreased. On the other hand, when the temperature approaches $T = T_c$, P_s is reduced to zero. This will cause the SNE to vanish because the vanishing of P_s effectively restores the inversion symmetry of the spinon dispersion.

In addition, the peak of spin Nernst coefficient at a special temperature results from the competition between the enhancement of excited spinons engaging in transport and the reduction of the second-NN order parameter P_s and M_s as the temperature increases. The staggered field will weaken the spin Nernst coefficient in opposite to that of DMI, because the staggered field supports a collinear configuration, but DMI favors a perpendicular one between two second-NN spin polarizations. In reality, T_N could be finite due to a variety of effects neglected here, and the temperature dependence of the spin Nernst coefficient is expected to depend on the competition between these effects and the DMI, especially near T_N. Nevertheless, the spin Nernst coefficient is shown to change continuously with increasing h_{st}. This implies that the spin Nernst coefficient changes continuously at the magnetic transition temperature as long as it is the second-order transition.

C. The relation between magnons and spinons in antiferromagnets

We now explore the connection between the SNE in the PM phase and the SNE in the AFM phase. In the Schwinger boson picture, the transition from the PM to AFM phase takes place via the spinon condensation [36]. Take Fig. 3(b) as an example. As the temperature is lowered to the Néel temperature T_N, the spinons will condense into the $\alpha_\uparrow$ and $\beta_\downarrow$ modes. Consequently, the resulting state will have a macroscopic occupation of spin up (down) at A (B) sites, giving rise to the AFM order. At the same time, the two upper modes, $\alpha_\downarrow$ and $\beta_\uparrow$, will evolve into magnons. In fact, upon the spinon condensation, the order parameter M_{-s}^A vanishes, and the

dispersion of the $\alpha_\downarrow$ mode becomes

$$E_{\alpha\downarrow}(\boldsymbol{k}) = -\frac{D_2}{4}P_+^S g_A(\boldsymbol{k}) + \sqrt{(\mu + h_{st}/2)^2 - |J_1\chi_0 f(\boldsymbol{k})|^2} \,. \tag{20}$$

Comparing the above expression with that of magnons $E_m(\boldsymbol{k}) = SD_2 g_A(\boldsymbol{k}) + \sqrt{(J_1 S + h_{st})^2 - S^2 J_1^2 |f(\boldsymbol{k})|^2}$ [25, 26], we see that they share the basic algebraic structure. The slight difference is due to the incomplete condensation of spinons.

It is obvious that across the phase boundary between the PM and AFM phase, the symmetries relevant to the SNE, namely, the combined $\mathcal{TI}$ symmetry and the breaking of the spin rotational symmetry due to D_2 remains the same. Hence the SNE in both the PM and AFM phase has the same microscopic origin, as shown in Fig. 6.

IV. SUMMARY AND DISCUSSION

In summary, we have studied the pure SNE in the PM state on an antiferromagnetic honeycomb lattice with a second-NN DMI, using the Schwinger boson mean-field method. We found that the pairs of the combined $\mathcal{TI}$ conjugate modes of spinons support a transverse spin current without a transverse thermal current. Because of the competition between the short-range spin correlations, represented by the temperature-dependent mean-field order parameters, and spin fluctuations, represented by the thermal population of spinons, the spin Nernst coefficient shows a nontrivial temperature dependence for a rather simple model considered here. This might suggest that a paramagnetic insulator with AFM interaction of spins could serve as a spintronics device even above the magnetic transition temperature to generate or detect the spin current.

Before closing, we would like to discuss several issues left for future studies. Throughout this paper, we neglected the fluctuations from the mean-field solution. In fact, the Schwinger boson mean-field treatment is the result of the zeroth order of $O(1/N)$ in a large-N expansion of a spin $SU(N)$ model [34]. Rigorously speaking, the low energy part of fluctuations, i.e., the phase fluc-

tuation of order parameters, could couple with the $U(1)$ gauge field, the dynamics of which may exhibit a confined or deconfined phase. Exploring these effects of fluctuations on spin transport will be an interesting problem in the future [37, 38]. However, since our argument about the finite SNE in the PM state of the honeycomb AFM is based on the combined $\mathcal{TI}$ symmetry, our conclusion would not be altered in a qualitative manner.

We did not use the full projected symmetry group method to analyze the spinon Hamiltonian. Such analyses would be necessary for spin liquid systems at low temperatures described by fermionic spinons. On the other hand, for investigating the pure SNE at high temperatures, it is sufficient to consider only the combined $\mathcal{TI}$ symmetry based on the unprojected spinon wave function.

So far we have only considered the so-called intrinsic contribution to the spinon SNE due to the Berry curvature of the spinon bands. Similar to the anomalous Hall effect [39], there should be extrinsic effect due to the scattering between spinons and other relevant physical degrees of freedom such as phonons. We note that there is an analogous effect of electrons [40, 41] for which the impurity scattering has been discussed [42].

In real materials, such as transition-metal trichalcogenides, the situation is more complicated. In addition to the interactions described in Eq. (1), longer-range exchange interactions are present, stabilizing complex magnetic ordered states [43]. Furthermore, single-ion anisotropies and anisotropic exchange interactions could exist, making finite-temperature magnetic ordering possible even for the two-dimensional limit [44]. These effects not only require solving a set of self-consistent equations for many order parameters but also require extending the current formalism as demonstrated in Ref. [33]. For $S > 1/2$ systems, h_{st} is related to the single-ion anisotropy K_2 as $h_{st} \sim K_2(S - 1/2)/SM_z$ with $M_z = \sum_{s,s'}(\sigma_3)_{s,s'}\langle c_{i,s}^\dagger c_{i,s'}\rangle$ [33]. For MnPS$_3$ as discussed in Ref. [25], h_{st}/J could become as large as 0.01 at low temperatures. This value is an order of magnitude smaller than the ones used in our analyses. Therefore, it is expected that the spin Nernst coefficient does not change significantly across a magnetic transition temperature. Detailed material dependence of the SNE including these effects is left for future studies.

Appendix A: Symmetry operations

We discuss symmetry operations on the spinon Hamiltonian in the momentum space. These symmetry operations include inversion operation $\mathcal{I}$, time reversal operation $\mathcal{T}$, and mirror operation $\mathcal{M}_z$.

The spinon Hamiltonian matrix at each $\boldsymbol{k}$ point is given by

$$H_s(\boldsymbol{k}) = \sum_\mu h_\mu^s(\boldsymbol{k})\sigma_\mu. \tag{A1}$$

For the inversion operation, we follow the definition of Eq. (6) in the lattice space, which ensures that $\mathcal{I}\boldsymbol{S}_{i,A(B)}\mathcal{I}^{-1} = \boldsymbol{S}_{-i,B(A)}$. Accordingly, the Hamiltonian matrix $H_s(\boldsymbol{k})$ is transformed as

$$\mathcal{I}H_s(\boldsymbol{k})\mathcal{I}^{-1} = \sigma_2 H_{-s}^T(\boldsymbol{k})\sigma_2. \tag{A2}$$

where T stands for the matrix transposition.

The time reversal operator $\mathcal{T}$ is defined in Eq. (5), and transforms $H_s(\boldsymbol{k})$ into

$$\mathcal{T}H_s(\boldsymbol{k})\mathcal{T}^{-1} = \sigma_3 H_{-s}^*(-\boldsymbol{k})\sigma_3. \tag{A3}$$

Under the combined $\mathcal{TI}$ operation, $H_s(\boldsymbol{k})$ is thus transformed as

$$\mathcal{TI}H_s(\boldsymbol{k})(\mathcal{TI})^{-1} = \sigma_1 H_s(-\boldsymbol{k})\sigma_1. \tag{A4}$$

Therefore, if the system has the combined $\mathcal{TI}$ symmetry, then $H_s(\boldsymbol{k})$ should satisfy

$$\sigma_1 H_s(-\boldsymbol{k})\sigma_1 = H_s(\boldsymbol{k}) . \tag{A5}$$

The mirror symmetry operator $\mathcal{M}_z$ with respect to the lattice plane is defined as

$$\mathcal{M}_z c_{i,s}\mathcal{M}_z^{-1} = i(\sigma_3)_{s,s'}c_{i,s'}, \tag{A6}$$

which leads to $\mathcal{M}_z S_i^z \mathcal{M}_z^{-1} = S_i^z$ and $\mathcal{M}_z S_i^{x,y}\mathcal{M}_z^{-1} = -S_i^{x,y}$. The Hamiltonian matrix is invariant under mirror operation $\mathcal{M}$

$$\mathcal{M}H_s(\boldsymbol{k})\mathcal{M}^{-1} = H_s(\boldsymbol{k}) . \tag{A7}$$

Appendix B: Mean-field self-consistent equations

The mean-field order parameters and the Lagrange multiplier μ are determined by minimizing the free energy involving these parameters. By differentiating the free energy with respect to these parameters and equating to zero, one arrives at the following set of self-consistent

equations:

$$1+2S = \frac{1}{2N}\sum_{\boldsymbol{k}s}\left[\frac{h_0^s(\boldsymbol{k})}{h^s(\boldsymbol{k})}(n_{\boldsymbol{k},s}^\alpha + n_{-\boldsymbol{k},-s}^\beta + 1)\right], \quad \text{(B1a)}$$

$$4\chi_0 = \frac{J_1\chi_0}{3N}\sum_{\boldsymbol{k}s}\left[\frac{|f(\boldsymbol{k})|^2}{h^s(\boldsymbol{k})}(n_{\boldsymbol{k},s}^\alpha + n_{-\boldsymbol{k},-s}^\beta + 1)\right], \quad \text{(B1b)}$$

$$M_s^A = \frac{1}{6N}\sum_{\boldsymbol{k}}g_A(\boldsymbol{k})(n_{\boldsymbol{k},s}^\alpha - n_{-\boldsymbol{k},-s}^\beta - 1), \quad \text{(B1c)}$$

$$-P_s^S = \frac{1}{6N}\sum_{\boldsymbol{k}}g_S(\boldsymbol{k})\frac{h_0^s(\boldsymbol{k})}{h^s(\boldsymbol{k})}(n_{\boldsymbol{k},s}^\alpha + n_{-\boldsymbol{k},-s}^\beta + 1), \quad \text{(B1d)}$$

where $n_{\boldsymbol{k},s}^{\alpha/\beta} = [\exp(E_{\alpha,\beta}^s(\boldsymbol{k})/T)-1]^{-1}$ is the Bose distribution function, and N is the number of unit cells.

Appendix C: BdG equation and Berry curvature

In this section we present a detailed discussion of the bosonic BdG equation and the associated wave functions. Our starting point is the spinon mean-field Hamiltonian (8), reproduced here for convenience,

$$H = \sum_{\boldsymbol{k},s}\Psi_{\boldsymbol{k}s}^\dagger H_s(\boldsymbol{k})\Psi_{\boldsymbol{k}s}, \quad \text{(C1)}$$

where $\Psi_{\boldsymbol{k}s} = [a_{\boldsymbol{k},s}, b_{-\boldsymbol{k},-s}^\dagger]^T$ with $a_{\boldsymbol{k},s}$ and $b_{\boldsymbol{k},s}$ being the Fourier transform of the spinon operators on the A and B sublattices, respectively. Introduce the Bogoliubov transformation

$$\begin{pmatrix} a_{\boldsymbol{k},s} \\ b_{-\boldsymbol{k},-s}^\dagger \end{pmatrix} = U_s(\boldsymbol{k})\begin{pmatrix} \alpha_{\boldsymbol{k},s} \\ \beta_{-\boldsymbol{k},-s}^\dagger \end{pmatrix}. \quad \text{(C2)}$$

The boson commutation relation dictates that $U_s(\boldsymbol{k})$ is a paraunitary matrix, i.e.,

$$U_s(\boldsymbol{k})\sigma_3 U_s^\dagger(\boldsymbol{k}) = \sigma_3. \quad \text{(C3)}$$

By demanding that the Bogoliubov transformation diagonalizes the Hamiltonian, i.e., $H = \sum_{\boldsymbol{k}s}[E_\alpha^s(\boldsymbol{k})\alpha_{\boldsymbol{k}s}^\dagger\alpha_{\boldsymbol{k}s} + E_\beta^{-s}(\boldsymbol{k})\beta_{\boldsymbol{k}s}^\dagger\beta_{\boldsymbol{k}s}]$, we obtain the BdG equation

$$H_s(\boldsymbol{k})U_s(\boldsymbol{k}) = \sigma_3 U_s(\boldsymbol{k})\sigma_3\Delta(\boldsymbol{k}), \quad \text{(C4)}$$

where $\Delta(\boldsymbol{k}) = \text{diag}(E_\alpha^s(\boldsymbol{k}), E_\beta^{-s}(-\boldsymbol{k}))$ is the eigenvalue matrix. We note that both the excitation energies $E_\alpha^s(\boldsymbol{k})$ and $E_\beta^{-s}(-\boldsymbol{k})$ must be positive. Otherwise the mean-field solution is unphysical. The explicit expression of $U_s(\boldsymbol{k})$ is given Eq. (10).

For the purpose of calculating the Berry curvature, it is necessary to clarify what the wave function of a spinon quasiparticle is. Let us write $U_s(\boldsymbol{k}) = [u_\alpha^s(\boldsymbol{k}), u_{\bar\beta}^{-s}(-\boldsymbol{k})]$, where $u_\alpha^s(\boldsymbol{k})$ and $u_{\bar\beta}^{-s}(-\boldsymbol{k})$ are two-component column vectors. Inserting this expression into the BdG equation (C4), we have

$$H_s(\boldsymbol{k})u_\alpha^s(\boldsymbol{k}) = E_\alpha^s(\boldsymbol{k})\sigma_3 u_\alpha^s(\boldsymbol{k}), \quad \text{(C5a)}$$

$$H_s(\boldsymbol{k})u_{\bar\beta}^{-s}(-\boldsymbol{k}) = -E_\beta^{-s}(-\boldsymbol{k})\sigma_3 u_{\bar\beta}^{-s}(-\boldsymbol{k}). \quad \text{(C5b)}$$

It is clear that $u_\alpha^s(\boldsymbol{k})$ and $u_{\bar\beta}^{-s}(-\boldsymbol{k})$ are the wave functions of the quasiparticle $\alpha_{\boldsymbol{k},s}$ with positive energy $E_\alpha^s(\boldsymbol{k})$ and the quasihole $\beta_{-\boldsymbol{k},-s}$ with negative energy $-E_\beta^{-s}(-\boldsymbol{k})$, respectively. We have denoted the quasihole wave functions by the subscript $\bar\alpha$ or $\bar\beta$.

The above discussion suggests that to find the quasiparticle wave function of the $\beta_{-\boldsymbol{k},-s}$ mode, we just need to recast the spinon Hamiltonian in the basis $\tilde\Psi_{\boldsymbol{k}s} = [b_{\boldsymbol{k},s}, a_{-\boldsymbol{k},-s}^\dagger]^T$. To do that, we make use of the particle-hole conjugate operator, defined by

$$\mathcal{C}c_{i,s}\mathcal{C}^{-1} = c_{i,s}^\dagger. \quad \text{(C6)}$$

Acting $\mathcal{C}$ on the basis $\Psi_{\boldsymbol{k}s}$, we have

$$\mathcal{C}\Psi_{\boldsymbol{k}s}\mathcal{C}^{-1} = \sigma_1\begin{bmatrix} b_{\boldsymbol{k},-s} \\ a_{-\boldsymbol{k},s}^\dagger \end{bmatrix}. \quad \text{(C7)}$$

Consequently,

$$\tilde H_s(\boldsymbol{k}) = \mathcal{C}H_s(\boldsymbol{k})\mathcal{C}^{-1} = \sigma_1 H_s^*(-\boldsymbol{k})\sigma_1. \quad \text{(C8)}$$

We can then deduce that

$$u_{\bar\beta}^{-s}(\boldsymbol{k}) = \sigma_1 u_{\bar\beta}^{-s*}(\boldsymbol{k}). \quad \text{(C9)}$$

If the system has $\mathcal{TI}$ symmetry, according to Eq. (A4)

$$\tilde H_s(\boldsymbol{k}) = \sigma_1 H_s^*(-\boldsymbol{k})\sigma_1 = H_s^*(\boldsymbol{k}). \quad \text{(C10)}$$

Since $\tilde H_s(\boldsymbol{k})$ and $H_s^*(\boldsymbol{k})$ describe the same physical system, we have

$$u_\beta^{-s}(\boldsymbol{k}) = u_\alpha^{s*}(\boldsymbol{k}). \quad \text{(C11)}$$

Appendix D: The property of Berry Curvature

The Berry curvature is generally defined by the projection operator

$$\Omega_n(\boldsymbol{k}) = -i\epsilon^{ij}\text{Tr}[\bar P_n(\boldsymbol{k})\partial_{k_i}P_n(\boldsymbol{k})\partial_{k_j}P_n(\boldsymbol{k})], \quad \text{(D1)}$$

where $P_n(\boldsymbol{k})$ is the projection operator for the n-th band at the momentum $\boldsymbol{k}$, and $\bar P_n \equiv 1 - P_n$. Note that for the generalized eigenvalue problem given by Eq. (C5), the projector operator is defined by [19]

$$P_n = \frac{|n\rangle\langle n|\sigma_3}{\langle n|\sigma_3|n\rangle}. \quad \text{(D2)}$$

For our disordered AFM described by the bosonic BdG Hamiltonian $H_s(\boldsymbol{k})$, this leads to the formula

$$\Omega_\lambda^s(\boldsymbol{k}) = i\partial_{\boldsymbol{k}}u_\lambda^{s\dagger}(\boldsymbol{k})\times\sigma_3\partial_{\boldsymbol{k}}u_\lambda^s(\boldsymbol{k})/(u_\lambda^{s\dagger}(\boldsymbol{k})\sigma_3 u_\lambda^s(\boldsymbol{k})), \quad \text{(D3)}$$

where $u_{\lambda,s}(\boldsymbol{k})$ is the wave function of λ-type quasiparticle or quasihole, and the normalization $u_{\lambda,s}^\dagger(\boldsymbol{k})\sigma_3 u_{\lambda,s}(\boldsymbol{k}) = \pm 1$ for quasiparticle and quasiholes, respectively.

For a two-level system, it follows from Eq. (D1) that the Berry curvature has the property

$$\Omega_n(\boldsymbol{k}) = -\Omega_{\bar{n}}(\boldsymbol{k}), \tag{D4}$$

where n and $\bar{n}$ refers to the quasiparticle and quasihole bands, respectively. This property is a special case of $\sum_n \Omega_n(\boldsymbol{k}) = 0$ with $n \geq 2$. Applying this relation to our Hamiltonian $H_s(\boldsymbol{k})$, we have

$$\Omega_\alpha^s(\boldsymbol{k}) = -\Omega_{\bar{\beta}}^{-s}(-\boldsymbol{k}). \tag{D5}$$

Using Eq. (C9), one can deduce the relation

$$\Omega_{\bar{\beta}}^{-s}(\boldsymbol{k}) = -\Omega_{\bar{\beta}}^{-s}(\boldsymbol{k}). \tag{D6}$$

The result can be also applied to a general reduced BdG Hamiltonian.

In the presence of the $\mathcal{TI}$ symmetry, the Berry curvatures for the two modes α and β could be also related. Using Eq. (C11), we find

$$\Omega_\alpha^s(\boldsymbol{k}) = -\Omega_\beta^{-s}(\boldsymbol{k}). \tag{D7}$$

[1] K. Uchida, S. Takahashi, K. Harii, J. Ieda, W. Koshibae, K. Ando, S. Maekawa, and E. Saitoh, "Observation of the spin seebeck effect," Nature **455**, 778 EP – (2008).

[2] Ken-ichi Uchida, Hiroto Adachi, Takeru Ota, Hiroyasu Nakayama, Sadamichi Maekawa, and Eiji Saitoh, "Observation of longitudinal spin-seebeck effect in magnetic insulators," Applied Physics Letters **97**, 172505 (2010).

[3] K. Uchida, J. Xiao, H. Adachi, J. Ohe, S. Takahashi, J. Ieda, T. Ota, Y. Kajiwara, H. Umezawa, H. Kawai, G. E. W. Bauer, S. Maekawa, and E. Saitoh, "Spin seebeck insulator," Nature Materials **9**, 894 EP – (2010).

[4] E. Saitoh S. Maekawa, S. O. Valenzuela and T. Kimura, eds., *Spin Current* (Oxford University Press, 2012).

[5] Gerrit E. W. Bauer, Eiji Saitoh, and Bart J. van Wees, "Spin caloritronics," Nature Materials **11**, 391 EP – (2012).

[6] Yuichi Ohnuma, Hiroto Adachi, Eiji Saitoh, and Sadamichi Maekawa, "Spin seebeck effect in antiferromagnets and compensated ferrimagnets," Phys. Rev. B **87**, 014423 (2013).

[7] T. Kikkawa, K. Uchida, Y. Shiomi, Z. Qiu, D. Hou, D. Tian, H. Nakayama, X.-F. Jin, and E. Saitoh, "Longitudinal spin seebeck effect free from the proximity nernst effect," Phys. Rev. Lett. **110**, 067207 (2013).

[8] A. V. Chumak, V. I. Vasyuchka, A. A. Serga, and B. Hillebrands, "Magnon spintronics," Nat Phys **11**, 453–461 (2015).

[9] L. J. Cornelissen, J. Liu, R. A. Duine, J. Ben Youssef, and B. J. van Wees, "Long-distance transport of magnon spin information in a magnetic insulator at room temperature," Nat Phys **11**, 1022–1026 (2015).

[10] Chui-Zhen Chen, Qing-feng Sun, Fa Wang, and X. C. Xie, "Detection of spinons via spin transport," Phys. Rev. B **88**, 041405 (2013).

[11] Hosho Katsura, Naoto Nagaosa, and Patrick A. Lee, "Theory of the thermal hall effect in quantum magnets," Phys. Rev. Lett. **104**, 066403 (2010).

[12] Y. Onose, T. Ideue, H. Katsura, Y. Shiomi, N. Nagaosa, and Y. Tokura, "Observation of the magnon hall effect," Science **329**, 297–299 (2010).

[13] Max Hirschberger, Robin Chisnell, Young S. Lee, and N. P. Ong, "Thermal hall effect of spin excitations in a kagome magnet," Phys. Rev. Lett. **115**, 106603 (2015).

[14] Max Hirschberger, Jason W. Krizan, R. J. Cava, and N. P. Ong, "Large thermal hall conductivity of neutral spin excitations in a frustrated quantum magnet," Science **348**, 106–109 (2015).

[15] T. Ideue, T. Kurumaji, S. Ishiwata, and Y. Tokura, "Giant thermal hall effect in multiferroics," Nature Materials **16**, 797 EP – (2017).

[16] Ryo Matsumoto and Shuichi Murakami, "Theoretical prediction of a rotating magnon wave packet in ferromagnets," Phys Rev Lett **106**, 197202 (2011).

[17] Ryo Matsumoto and Shuichi Murakami, "Rotational motion of magnons and the thermal hall effect," Phys. Rev. B **84**, 184406 (2011).

[18] Lifa Zhang, Jie Ren, Jian-Sheng Wang, and Baowen Li, "Topological magnon insulator in insulating ferromagnet," Phys. Rev. B **87**, 144101 (2013).

[19] Ryuichi Shindou, Ryo Matsumoto, Shuichi Murakami, and Jun-ichiro Ohe, "Topological chiral magnonic edge mode in a magnonic crystal," Phys. Rev. B **87**, 174427 (2013).

[20] Hyunyong Lee, Jung Hoon Han, and Patrick A. Lee, "Thermal hall effect of spins in a paramagnet," Phys. Rev. B **91**, 125413 (2015).

[21] Jung Hoon Han and Hyunyong Lee, "Spin chirality and hall-like transport phenomena of spin excitations," *Journal of the Physical Society of Japan*, Journal of the Physical Society of Japan **86**, 011007 (2016).

[22] S. A. Owerre, "Topological honeycomb magnon hall effect: A calculation of thermal hall conductivity of magnetic spin excitations," Journal of Applied Physics **120**, 043903 (2016).

[23] S. A. Owerre, "Magnon hall effect in ab-stacked bilayer honeycomb quantum magnets," Phys. Rev. B **94**, 094405 (2016).

[24] S. A. Owerre, "Topological thermal hall effect in frustrated kagome antiferromagnets," Phys. Rev. B **95**, 014422 (2017).

[25] Ran Cheng, Satoshi Okamoto, and Di Xiao, "Spin nernst effect of magnons in collinear antiferromagnets," Phys. Rev. Lett. **117**, 217202 (2016).

[26] Vladimir A. Zyuzin and Alexey A. Kovalev, "Magnon spin nernst effect in antiferromagnets," Phys. Rev. Lett. **117**, 217203 (2016).

[27] Ki Hoon Lee, Suk Bum Chung, Kisoo Park, and Je-Geun Park, "Magnonic quantum spin hall state in the zigzag

and stripe phases of the antiferromagnetic honeycomb lattice," Phys. Rev. B **97**, 180401 (2018).

[28] Se Kwon Kim, Héctor Ochoa, Ricardo Zarzuela, and Yaroslav Tserkovnyak, "Realization of the haldane-kane-mele model in a system of localized spins," Phys. Rev. Lett. **117**, 227201 (2016).

[29] Y. Shiomi, R. Takashima, and E. Saitoh, "Experimental evidence consistent with a magnon nernst effect in the antiferromagnetic insulator mnps$_3$," Phys. Rev. B **96**, 134425 (2017).

[30] I. Dzyaloshinsky, "A thermodynamic theory of "weak" ferromagnetism of antiferromagnetics," Journal of Physics and Chemistry of Solids **4**, 241 – 255 (1958).

[31] Tôru Moriya, "Anisotropic superexchange interaction and weak ferromagnetism," Phys. Rev. **120**, 91–98 (1960).

[32] While it is not easy to apply such a field externally, similar effects could arise when the SU(2) symmetry is broken by the single-ion anisotropy for $S > 1/2$ or the Ising-type anisotropy in the exchange coupling within a Schwinger boson mean-field approach [33]. This allows magnetic ordering in low-dimensional systems at finite temperature.

[33] Carsten Timm and P. J. Jensen, "Schwinger boson theory of anisotropic ferromagnetic ultrathin films," Phys. Rev. B **62**, 5634–5646 (2000).

[34] Assa Auerbach, *Interacting Electrons and Quantum Magnetism* (Springer-Verlag New York, 1994).

[35] Note that our definition of the $\mathcal{I}$ operator has an additional matrix σ_3. It flips the sign of the spinon operator on the B site, and is needed to make sure the NN bond term (χ_{ij}) transform into itself under the $\mathcal{TI}$ operation. The σ_3 matrix is allowed since there is an extra phase freedom in the spinon representation.

[36] Sanjoy Sarker, C. Jayaprakash, H. R. Krishnamurthy, and Michael Ma, "Bosonic mean-field theory of quantum heisenberg spin systems: Bose condensation and magnetic order," Phys. Rev. B **40**, 5028–5035 (1989).

[37] N. Read and Subir Sachdev, "Large-n expansion for frustrated quantum antiferromagnets," Phys. Rev. Lett. **66**, 1773–1776 (1991).

[38] Yi Zhou, Kazushi Kanoda, and Tai-Kai Ng, "Quantum spin liquid states," Rev. Mod. Phys. **89**, 025003 (2017).

[39] Naoto Nagaosa, Jairo Sinova, Shigeki Onoda, A. H. MacDonald, and N. P. Ong, "Anomalous hall effect," Rev. Mod. Phys. **82**, 1539–1592 (2010).

[40] V. P. Gusynin, S. G. Sharapov, and A. A. Varlamov, "Anomalous thermospin effect in the low-buckled dirac materials," Phys. Rev. B **90**, 155107 (2014).

[41] V. P. Gusynin, S. G. Sharapov, and A. A. Varlamov, "Spin nernst effect and intrinsic magnetization in two-dimensional dirac materials," *Low Temperature Physics*, Low Temperature Physics **41**, 342–352 (2015).

[42] A. Dyrdał, J. Barnaś, and V. K. Dugaev, "Spin hall and spin nernst effects in a two-dimensional electron gas with rashba spin-orbit interaction: Temperature dependence," Phys. Rev. B **94**, 035306 (2016).

[43] Nikhil Sivadas, Matthew W. Daniels, Robert H. Swendsen, Satoshi Okamoto, and Di Xiao, "Magnetic ground state of semiconducting transition-metal trichalcogenide monolayers," Phys. Rev. B **91**, 235425 (2015).

[44] Bevin Huang, Genevieve Clark, Efrén Navarro-Moratalla, Dahlia R. Klein, Ran Cheng, Kyle L. Seyler, Ding Zhong, Emma Schmidgall, Michael A. McGuire, David H. Cobden, Wang Yao, Di Xiao, Pablo Jarillo-Herrero, and Xiaodong Xu, "Layer-dependent ferromagnetism in a van der waals crystal down to the monolayer limit," Nature **546**, 270 EP – (2017).